# Moiré Fringe Signal Subdivision System of a Stained Code Disc of a Grating Displacement Sensor

Changhai Zhao, *Member, IEEE*, Qiuhua Wan, Xinran Lu, and Lihui Liang

***Abstract*—When a code disk of a displacement sensor is exposed to dust or other impurities, it causes distortion of the grating moiré fringe signal, and thereby provides wrong displacement information from the sensor. Therefore, it is necessary to analyze the distortion in the reading due to the stains. In this paper, multiple reading heads were used to collect the moiré fringe signal of the sensor and were evenly distributed on the fine code channel. Each reading head was used to subdivide the moiré fringe signal collected by it, calculate the signal amplitude value corresponding to each sampling point, and analyze the stains of the code disk corresponding to the reading head according to the signal amplitude value. According to the stains of the code disk, the subdivision value of each reading head was considered to have a certain weight. It was found that when the reading head is stained, the weight decreases, whereas when it is clean, the weight increases. Finally, the weighted average value of the two reading heads was taken as the final subdivision value of the sensor. The experimental results showed that the system provides output with high-precision displacement values even when the moiré fringe signal was abnormal due to the local stains of the sensor's code disk, therefore it significantly increases the anti-stain ability of the sensor.**

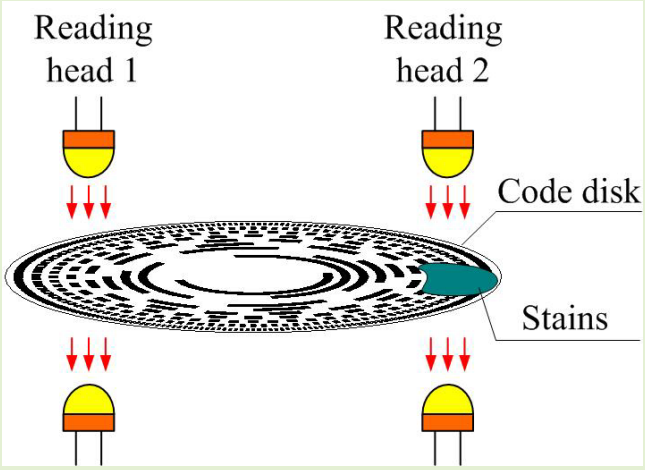


***Index Terms*— Displacement sensor, stained code disc, subdivision value, Moiré fringe.**

## I. Introduction

IN HIGH-PRECISION displacement sensors, the grating moiré fringe subdivision technology is mostly used to obtain displacement information [1]–[3]. Due to the limited technical level of the current grating scribing accuracy, equipment manufacturing, and assembly and adjustment technology, it is difficult to achieve high-precision and high-resolution measurement using the displacement sensors with higher-precision grating code discs. Therefore, the subdivision technology of the photoelectric moiré fringe signal is used to improve the resolution and accuracy of the displacement sensors. The quality of the photoelectric moiré fringe signal directly affects the subdivision accuracy and the measurement accuracy of the sensor [4]–[8].

Since the displacement sensor is a moving part, it is impossible to completely seal it during operation. When used in harsh environments, the inner side of the sensor which consists of the code disk will inevitably be exposed to dust or other impurities. At times, when the external environment changes violently or the cooling system is operated at full speed, the condensation water will cause distortion of the moiré fringe signal and increase the subdivision error. Further, when the interpolation error is large, it leads to incorrect displacement data output by the displacement sensor. Presently, Fourier analysis and other methods are commonly used to measure the waveform parameters when the moiré fringe signal is distorted. Then, the interpolation error is calculated based on the waveform parameters of the signal, and the error compensation is performed in order to improve the accuracy of the displacement sensor [9]–[15]. By this method, it is possible to have a good effect on a stable moiré fringe signal, however when the code disk of the sensor is locally stained,

Manuscript received March 6, 2022; accepted March 27, 2022. Date of publication March 31, 2022; date of current version April 29, 2022. This work was supported in part by the National Natural Science Foundation of China under Grant 52075520 and in part by the Science and Technology Development Programme of Jilin Province under Grant 20210201097GX. The associate editor coordinating the review of this article and approving it for publication was Prof. Kea-Tiong (Samuel) Tang. *(Corresponding author: Changhai Zhao.)*

The authors are with the Changchun Institute of Optics, Fine Mechanics and Physics, Chinese Academy of Sciences, Changchun 130033, China (e-mail: zhaoch@ciomp.ac.cn).

Digital Object Identifier 10.1109/JSEN.2022.3163732

1558-1748 © 2022 IEEE. Personal use is permitted, but republication/redistribution requires IEEE permission.
See https://www.ieee.org/publications/rights/index.html for more information.

Authorized licensed use limited to: Changchun Inst of Optics Fine Mechanics & Physics. Downloaded on February 07,2023 at 02:30:04 UTC from IEEE Xplore. Restrictions apply.

and the stained part passes through the sensor's reading head, the moiré fringe signal would change drastically. Moreover, by using the compensation algorithm, its effect would become insignificant, or even counterproductive.

In this work, two reading heads were used to read the fine code information of the displacement sensor. The two reading heads were diametrically installed at both ends of the code disk and were used to collect the moiré fringe signals respectively. It was found that when the code disc was clean, the signal output from each reading head was a stable moiré fringe signal, and the signal amplitudes corresponding to the same subdivision points of different signal periods were consistent. When there were stains on the code disk, it will leads to uneven transmittance. The signal amplitudes corresponding to the same subdivision points of different moiré signal periods were different. According to the deviation between the amplitude value of the moiré fringe signal and the standard amplitude value, the stains of the code disk was judged, and then the subdivision value of each reading head was considered to have a certain weight. Then, the final subdivision angle value of the sensor is the weighted average of the two reading heads. When the reading head is clean at a certain position, its weight is 1, and is 0 when it is seriously stained. When the weight is 0, this position does not participate in the final angle calculation. By using this algorithm, serious stained reading head could be prevented to participate in the final displacement calculation, and could ensure that when the code disk has local stains, the sensor could produce an output with high displacement accuracy. As long as the code disc positions of the two reading heads are not severely stained, the sensor could produce an output with a high-precision displacement value.

This technology is mainly used for displacement sensors working in harsh environment. For example, mobile radars often working in the field, mobile measuring equipment and measuring ships working on the ocean.

## II. Characteristics of the Moiré Fringe Signal

### A. Hardware Schematic

The optical fringe formed by the superposition of the two periodic grating patterns with similar spatial frequencies is called moiré fringe. Moiré fringes amplify the grating based on the precise measurement of the grating displacement [16]. At present, the grating moiré fringe signal subdivision method is mostly used to obtain high-precision displacement data.

The displacement sensors are classified into angular displacement sensors and linear displacement sensors. The angular displacement sensor uses a circular grating, whereas the linear displacement sensor uses a linear grating. In this work, the circular grating was used as the research object. Initially, two reading heads were used to collect the moiré fringe signals of the angular displacement sensor. The two reading heads were diametrically installed at both ends of the angular displacement sensor. Each reading head consists of four photosensitive elements. It was found that when the grating slit was carved, the phase difference of the slit corresponding to the four photosensitive elements was 90 degrees. Moreover, when the sensor works, each reading head provided outputs through the four channels of the original fine code moiré fringe signals. The four signals were quasi sinusoidal signals with a phase difference of 90 degrees, which were recorded as J0, J90, J180, and J270 respectively. The phase of J0, J90, J180, and J270 were 0 degrees, 90 degrees, 180 degrees, and 270 degrees respectively. J0 and J180 enter the "+" pin and "−" pin of the amplifier respectively, and the output signal after differential amplification was recorded as SIN. Similarly, J90 and J270 also enter the "+" pin and "−" pin of the amplifier respectively, and the signal after differential amplification was recorded as COS. The signals output by the two reading heads were the same, which implies that each reading head provides two amplified SIN and COS signals. The principle of signal acquisition is shown in Fig. 1.

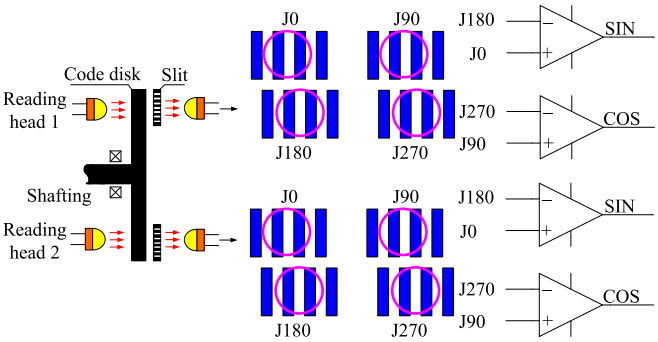


Fig. 1. Schematic diagram of signal acquisition.

### B. Signal Characteristics of a Clean Code Disc

The principle of the displacement sensor subdivision was derived from the formula $\tan\theta = \sin\theta/\cos\theta$, where $\theta$ is the theoretical value of the subdivision angle, $\sin\theta$ is the signal SIN amplified by the difference between J0 and J180 output by the reading head, and $\cos\theta$ is the differentially amplified signal COS of J90 and J270. Due to the existence of various errors, the two signals SIN and COS after differential amplification of the sensor were quasi-sine wave signals, which were represented by the Fourier series as shown in (1):

$$\begin{cases} U_a = a_0 + a_1 \cdot \sin(\theta+\phi) + \sum_{i=2}^{\infty} a_i \cdot \sin(i\theta+\phi_{ia}) + \delta_e \\ U_b = b_0 + b_1 \cdot \cos(\theta+\phi_b) + \sum_{i=2}^{\infty} b_i \cdot \cos(i\theta+\phi_{ib}) + \delta_e \end{cases} \tag{1}$$

where $U_a$ corresponds to the SIN signal of the reading head, and $U_b$ corresponds to COS, $a_0$ and $b_0$ are the direct components of the signal, which are the sources of the DC component error; $a_1$ and $b_1$ are the amplitudes of the fundamental signals, which are the sources of the signal amplitude error; $\phi$ and $\phi_b$ are the fundamental phases of $U_a$ and $U_b$, the phase difference of the two signals is the source of phase error; $\sum_{i=2}^{\infty} a_i \cdot \sin(i\theta+\phi_{ia})$ and $\sum_{i=2}^{\infty} b_i \cdot \cos(i\theta+\phi_{ib})$ are the sum of higher harmonic components, which are the sources of harmonic component errors; and $\delta_e$ is the electrical noise, which is the source of noise error.

The figure formed with the SIN and COS signals as the abscissa and ordinate is a Lissajous figure. When the

Authorized licensed use limited to: Changchun Inst of Optics Fine Mechanics & Physics. Downloaded on February 07,2023 at 02:30:04 UTC from IEEE Xplore. Restrictions apply.

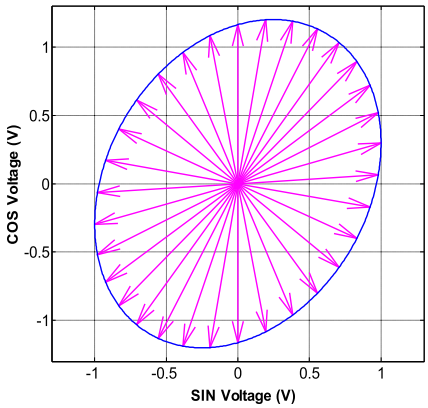


Fig. 2. Lissajous graph of a clean code disk.

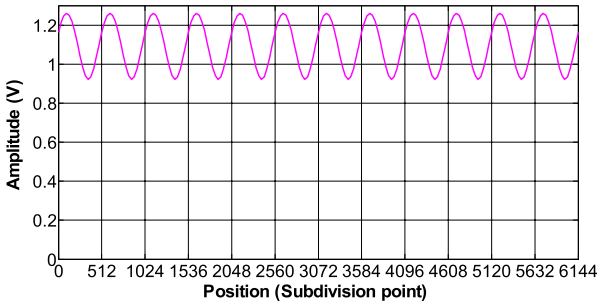


Fig. 3. Graph of subdivision value and amplitude value.

displacement sensor is installed and adjusted, the method of observing the Lissajous figure is often used to judge the quality of the signal. The standard Lissajous figure is a circle. When the code disk of the sensor is clean, the moiré fringe signal output that is obtained from the sensor is approximated as a stable signal. The Lissajous graph formed by the two amplified signals SIN and COS is stable, which implies that the Lissajous graphs formed by different moiré fringe signal periods have the same shape, as shown in Fig. 2.

When the two amplified moire fringe signals collected by the sensing reading head at a certain position $x$ are $U_{ax}$ and $U_{bx}$, then the subdivision value of the position is obtained as shown in (2):

$$\theta_x = \tan^{-1}(\frac{U_{ax}}{U_{bx}}) \tag{2}$$

The amplitude value corresponding to the subdivision value is obtained as shown in (3):

$$V_x = \sqrt{U_{ax}^2 + U_{bx}^2} \tag{3}$$

In different moiré fringe signal periods, when the subdivision value $\theta$ is the same, the corresponding amplitude value $V$ is also fixed. As shown in Fig. 3, the number of subdivisions of each moiré fringe signal period is 1024.

### C. Signal Characteristics of a Stained Code Disk

When the encoder of the sensor is stained, the moiré fringes obtained from the reading head of the sensor are unstable

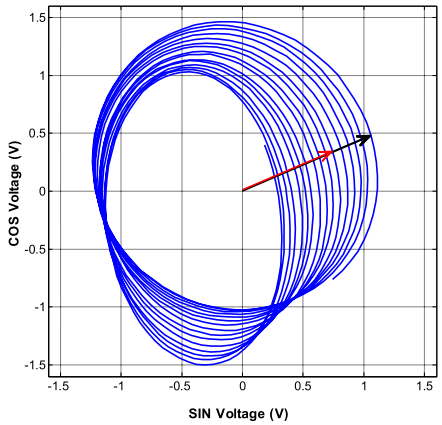


Fig. 4. Lissajous graph of a stained code disk.

signals due to the irregular shape of the stains. The shapes of the Lissajous figures corresponding to different signal periods are different. As shown in Fig. 4, the amplitude values corresponding to different signal periods at the same subdivision position are different. At this time, if the conventional error compensation algorithm is used to calculate the subdivision value, then it leads to a large error, which implies that the sensor cannot be used.

## III. Subdivision Algorithm of the Moiré Fringe Signal

When the code disk is clean, assuming that the standard vector amplitude value of the moiré fringe signal of the displacement sensor calculated using (3) at a subdivision point is $V_{REF}$, and the actual vector amplitude value calculated at the subdivision point is $V_{REAL}$, the amplitude error of the signal at the subdivision point is expressed as shown in (4):

$$E = \left| \frac{V_{REAL} - V_{REF}}{V_{REF}} \right| \tag{4}$$

In equation (4), when $E = 0$, it indicates that the amplitude value at the subdivision point is consistent with the standard vector amplitude value, and the code disc of the sensor is considered clean. The larger the value, the more serious the stain. When the signal amplitude of the moiré fringe changes within a small range, it will not have a substantial impact on the accuracy of the sensor, which is usually ignored. In order to ensure that the displacement value obtained from the sensor does not jump during the actual calculations, the allowable range of the signal amplitude error is considered to be between $E_{MIN}$ and $E_{MAX}$. Furthermore, when the amplitude error of a reading head at a subdivision position is less than $E_{MIN}$, that is, $E < E_{MIN}$, it is considered that the reading head is clean at that position, and the weight coefficient of the reading head is $W = 1$. When the amplitude error is greater than $E_{MAX}$, the reading head is severely stained at this position, that is, $E > E_{MAX}$ and the weight coefficient of the reading head is $W = 0$. Moreover, when the amplitude error is in the middle of the maximum and minimum values, that is, $E_{MIN} \leq E \leq E_{MAX}$, the weight coefficient of the group of the reading heads

Authorized licensed use limited to: Changchun Inst of Optics Fine Mechanics & Physics. Downloaded on February 07,2023 at 02:30:04 UTC from IEEE Xplore. Restrictions apply.

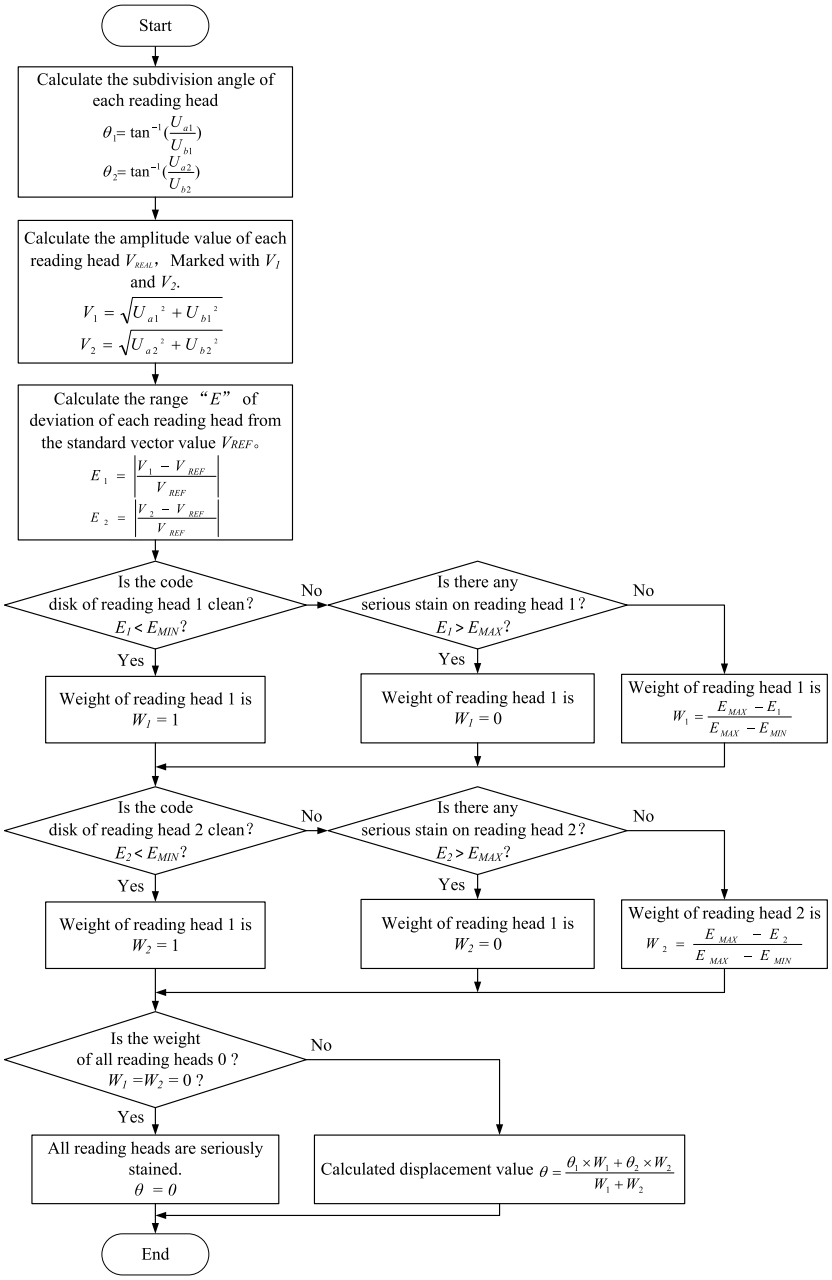


Fig. 5. The flow chart of algorithm.

is expressed as shown in (5):

$$W = \frac{E_{MAX} - E}{E_{MAX} - E_{MIN}} \tag{5}$$

If a displacement sensor has a total of $n$ groups of reading heads, the displacement value of the $i$ group of reading heads after the moiré fringe signal is subdivided is $\theta_i$, and the weight coefficient of the reading head is $W_i$, then the final output displacement value of the displacement sensor is obtained as shown in (6):

$$\theta = \frac{\sum_{i=1}^{n} \theta_i \times W_i}{\sum_{i=1}^{n} W_i} \tag{6}$$

From equation (6), it is observed that as long as the weight coefficient of any group of the reading heads of the displacement sensor is not zero, the displacement sensor provides an accurate correct displacement value. When a group of reading heads is severely stained, and when the amplitude error of all subdivision points in the whole moiré fringe signal period of the reading head is less than $E_{MAX}$, then the reading head is considered to move out of the stained area, and the group of reading heads participates in the final displacement calculations.

When the number of sensor reading heads is two, the algorithm flow chart is shown in Fig. 5, the $U_{a1}$ and $U_{b1}$ are SIN and COS signals of reading head 1, and $U_{a2}$ and $U_{b2}$ are signals of reading head 2.

Authorized licensed use limited to: Changchun Inst of Optics Fine Mechanics & Physics. Downloaded on February 07,2023 at 02:30:04 UTC from IEEE Xplore. Restrictions apply.

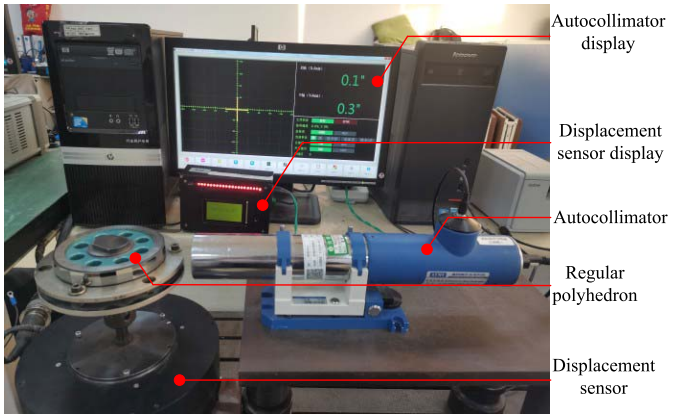


Fig. 6. Accuracy measurement diagram of angular displacement sensor.

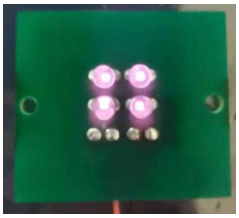

Fig. 7. Infrared light-emitting diode.

## IV. Experiment

By taking a 22-bit absolute angular displacement sensor as an example, the fine code trace of the sensor was taken as 4096 pairs of lines per cycle and the number of subdivisions of each moiré fringe signal cycle was taken as 1024. The corresponding angle of each fine code cycle was taken as 316.40625″ and the diameter of the code disc was taken as 160 mm. The sensor consists of two fine code reading heads, which were installed diametrically. Each reading head provides outputs through four channels of original fine code signals, which were amplified using a differential amplifier and converted into two channels of SIN and COS signals.

The accuracy measurement of the angular displacement sensor is shown in Fig. 6. While measuring, the angular displacement sensor and the regular polyhedron were connected coaxially, and turn the sensor, the autocollimator and the regular polyhedron were used as the angle references. The difference between the angle displayed value of the displacement sensor and the angle turned by the regular polyhedron was considered as the static error of the displacement sensor at the measuring point. Then, the angular displacement sensor was continued to rotate until all the measuring points were measured.

The infrared light-emitting diode of the displacement sensor is shown in Fig. 7, and the photoelectric receiving tube and the light-emitting diode are in one-to-one correspondence.

The code disk and slit of the sensor are shown in Fig. 8. When the sensor is working, the code disk rotates synchronously with the shaft system, and the slit is fixed. The code disk and slit are made in the same way. The manufacturing process is to evaporate a layer of chrome aluminum film on the glass, then apply photo resist, and then cover the

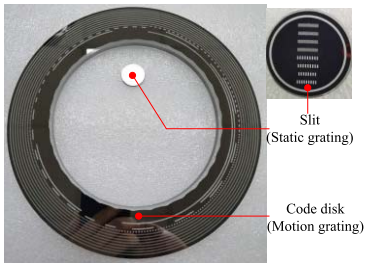


Fig. 8. Code disk and slit picture.

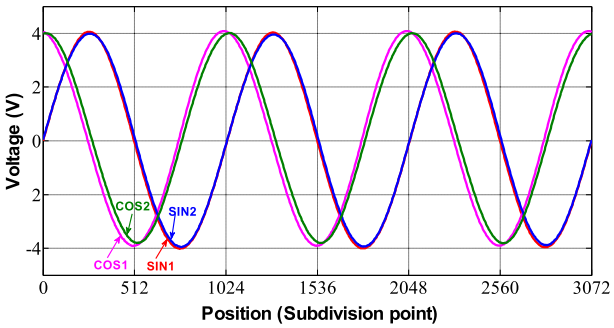


Fig. 9. Moiré fringe signal graph of reading head 1 and 2 when the code disk is clean. 'SIN1' and 'COS1' are the voltage values of reading head 1 collected when the sensor rotates. 'SIN1' corresponds to '$U_a$' and 'COS1' corresponds to '$U_b$' in equation (1). 'SIN2' and 'COS2' are the voltage values of reading head 2.

engraved motherboard on it for exposure. Then wash off the non photosensitive photo resist film, and then etch it with acid or alkali solution. After etching, wash off the photosensitive photo resist film, and then the code disk pattern is completed.

In the subdivision calculation of the sensor, the subdivision displacement of each reading head was calculated using (2), and the average value of the subdivision displacement of the two reading heads was taken as the final subdivision displacement value. The moiré fringe signals output from reading heads 1 and 2 of the clean sensor code disc are shown in Fig. 9, which are signal graph of three complete periods. The resulting Lissajous graph is shown in Fig. 10, and the corresponding amplitude graph for each subdivision point is shown in Fig. 11. By taking the signal amplitude value of the first subdivision period as a reference, the amplitude error curve calculated according to (4) in the second and third periods is shown in Fig. 12.

By considering the 0° position of the angular displacement sensor as the research object, an autocollimator was used to measure the error of the sensor in a subdivision period at 0° position. The error curve is shown in Fig. 13. In Fig. 13, the starting point of the subdivision period is taken as the origin, and the error of the origin is zero. It is observed that when there was only reading head 1, the peak value of error was 4.0″, the valley value was −0.2″, and the mean square error was 1.33″. It was also observed that when only reading head 2 was considered, the peak value of error was 1.1″, the valley value was −7.8″, and the mean square error was 2.45″. When the data of reading head 1 and reading head 2 were averaged, the peak value of error, the valley value, and the

Authorized licensed use limited to: Changchun Inst of Optics Fine Mechanics & Physics. Downloaded on February 07,2023 at 02:30:04 UTC from IEEE Xplore. Restrictions apply.

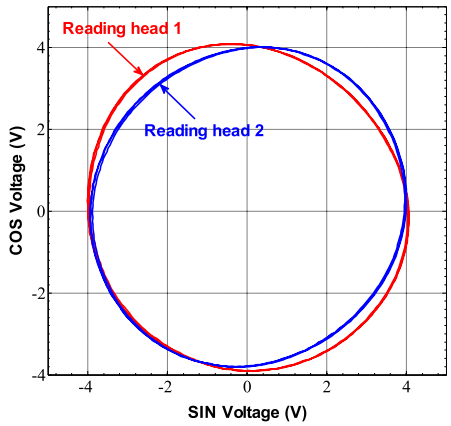


Fig. 10. Experimental Lissajous graph of the clean code disk.

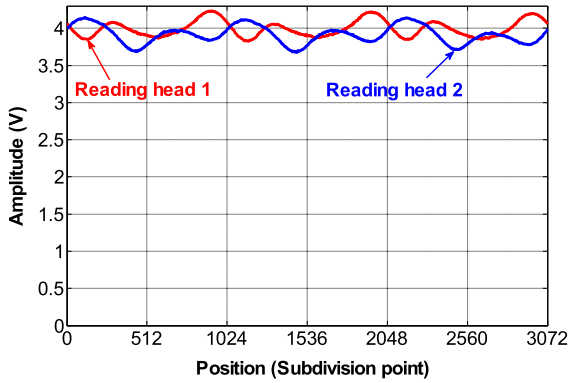


Fig. 11. Signal amplitude graph. The amplitude value is the result calculated by equation (3), including three complete signal periods.

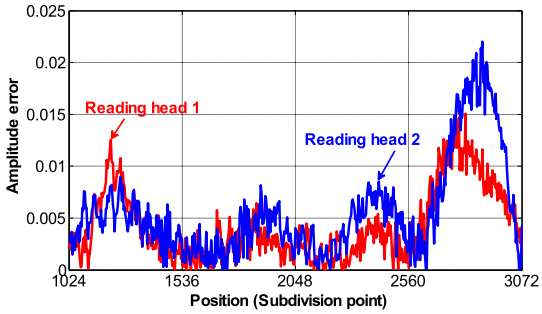


Fig. 12. Amplitude error curve. The amplitude error value is the value calculated by equation (4) and takes the amplitude value of the first signal period as the reference signal. Amplitude error is a relative value without unit.

mean square error were 1.3″, −3.9″, and 1.46″ respectively. For most displacement sensors, the average accuracy of two reading heads is higher than that of a single reading head. However, there are a few positions where the average accuracy of the reading head is lower than that of a certain reading head but higher than that of the worst reading head.

Simulate the condensate formed at the actual working site of the sensor and drip the water into the code disk to form stains, as shown in Fig. 14. When there was stains on the code disk and the reading head 1 was in the stained area

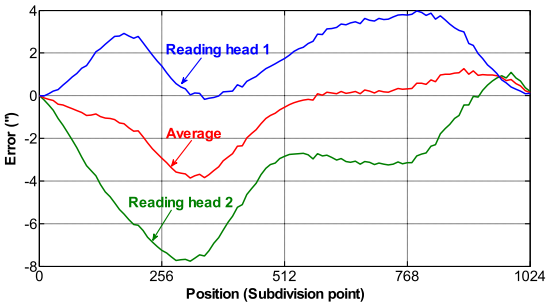


Fig. 13. Subdivision error graph. Subdivision error is the value of a complete moiré signal period measured by the method of Fig. 5.

Fig. 14. Code disk stain.

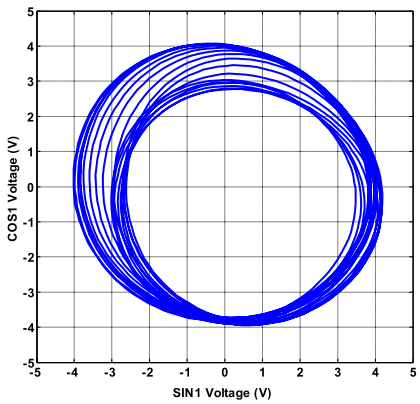


Fig. 15. Experimental Lissajous figure of the stained code disk.

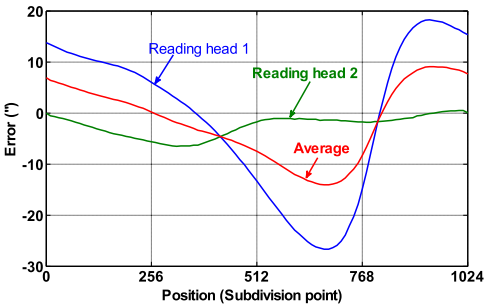


Fig. 16. Subdivision error graph of the stained code disk.

on the code disk, the obtained Lissajous figure is shown in Fig. 15. When the average value of the subdivision values of the two reading heads was taken as the output value of the sensor, the interpolation error of a certain period of the sensor was calculated according to the waveform as shown in Fig. 16, which was calculated with the subdivision zero of the

Authorized licensed use limited to: Changchun Inst of Optics Fine Mechanics & Physics. Downloaded on February 07,2023 at 02:30:04 UTC from IEEE Xplore. Restrictions apply.

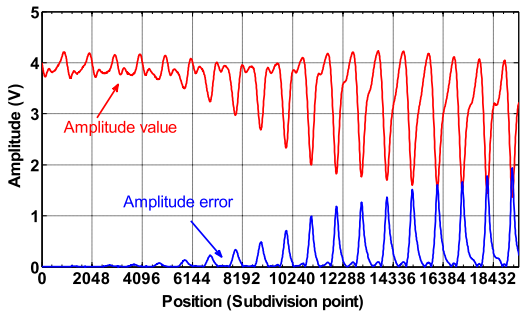


Fig. 17. Amplitude value and amplitude error graph of the stained code disk.

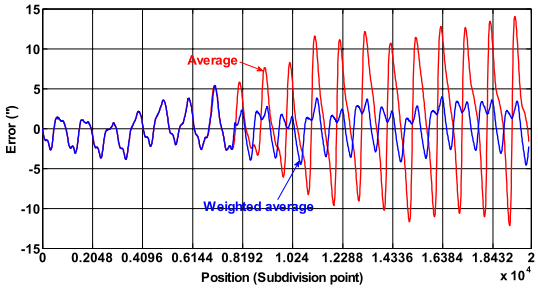


Fig. 18. Subdivision error graph of average value and the weighted average value.

reading head 2 as the origin, the peak value of the error, the valley value, and the mean square error was obtained as $9.1''$, $-14.1''$, and $7.4''$. The amplitude value of the signal at the same subdivision point was compared with the amplitude value when it was not stained, and its amplitude and amplitude error is shown in Fig. 17. With the further aggravation of stains, the subdivision error of the sensor would be further aggravated, which would directly cause the sensor to provide wrong results and it could not be used.

From Fig. 17, it is observed that even if the reading head of the sensor was in the heavily stained area, the amplitude error value was very insignificant, whereas the subdivision value had a large error, and the current data would be discarded. It is also observed that, in the actual calculations of the system, when the reading head entered the seriously stained area of the code disk, the weight coefficient of the reading head was 0. When the amplitude error obtained from the reading head in a complete subdivision period was lesser than the maximum allowable range, the reading head was considered to have moved out of the severely stained area of the code disk, and the weight coefficient of the reading head was greater than 0. Assuming that $E_{MAX} = 0.2$ and $E_{MIN} = 0.1$, according to (6), when the reading head entered the stained area of the code disk from the clean area, the calculated subdivision error curve is shown in Fig. 18. When the sensor was rotated, the displacement value obtained from the sensor was continuous displacement data, and the maximum subdivision error was the maximum error of the reading head 2 which was not in the stained area. It was found that when this algorithm was not used, with the increase of stains, the error of the sensor became larger and eventually lead to the wrong code of the sensor. When this algorithm was used, when the code disk of the sensor was stained locally, the sensor was found to maintain high output accuracy.

It is difficult to quantify the degree of stains on various code discs. In actual use, different stain thresholds need to be set according to the stain condition to make the system work normally. For example, when the system is used for radar tracking the target, when the code disk is stained, the error of the sensor will be relatively large, and the target may not be tracked effectively. At this time, the appropriate stain threshold can be set as needed to make the tracking effect meet the requirements. Deformation of the encoder disc, geometric eccentricity, and jitter caused by temperature drift can all lead to a decrease in sensor accuracy. However, since a certain margin is reserved in advance, the change in accuracy is within the design range and does not affect the normal operation of the sensor.

## V. Conclusion

In this work, two opposite diameter mounted reading heads were used to collect the fine code moiré fringe signals of angular displacement sensors, and the subdivision displacement value and corresponding amplitude value were calculated in order to judge whether the code disk at the corresponding position of the reading head was stained. Based on the severity of stains, a certain weight was assigned to the subdivision displacement value, and the weighted average of the subdivision values of the two reading heads was obtained as the final subdivision displacement value. It was found that, when the code disc of the sensor was locally stained, it results in a large subdivision error. This method was found to enable the sensor to provide a highly precise displacement value. In this paper, without adding any hardware, we only rely on the algorithm to reduce the error caused by the stain of the code disk, so as to increase the ability of the displacement sensor to adapt to the harsh environment.

## References

[1] L. Quan, Y. Shimizu, X. Xiong, H. Matsukuma, and W. Gao, "A new method for evaluation of the pitch deviation of a linear scale grating by an optical angle sensor," *Precis. Eng.*, vol. 67, pp. 1–13, Jan. 2021.

[2] G. Ye *et al.*, "Ratiometric-linearization-based high-precision electronic interpolator for sinusoidal optical encoders," *IEEE Trans. Ind. Electron.*, vol. 65, no. 10, pp. 8224–8231, Oct. 2018.

[3] C.-C. Hsu, H. Chen, C.-W. Chiang, and Y.-W. Chang, "Dual displacement resolution encoder by integrating single holographic grating sensor and heterodyne interferometry," *Opt. Exp.*, vol. 25, no. 24, pp. 30189–30202, Nov. 2017.

[4] S. Odinokov, M. Shishova, M. Kovalev, A. Zherdev, and D. Lushnikov, "Phase imbalance optimization in interference linear displacement sensor with surface gratings," *Sensors*, vol. 20, no. 5, p. 1453, Mar. 2020.

[5] J. Deng *et al.*, "Eightfold optical encoder with high-density grating," *Appl. Opt.*, vol. 57, no. 10, pp. 2366–2375, Apr. 2018.

[6] X. Li *et al.*, "A novel optical rotary encoder with eccentricity self-detection ability," *Rev. Sci. Instrum.*, vol. 88, no. 11, Nov. 2017, Art. no. 115005.

[7] X. Li *et al.*, "Two-probe optical encoder for absolute positioning of precision stages by using an improved scale grating," *Opt. Exp.*, vol. 24, no. 19, pp. 21378–21391, Sep. 2016.

[8] G. Ye *et al.*, "Optimal design of a reflective diffraction grating scale with sine-trapezoidal groove for interferential optical encoders," *Opt. Lasers Eng.*, vol. 134, Nov. 2020, Art. no. 106196.

[9] G. S. Miljkovic and D. B. Denic, "Redundant and flexible pseudorandom optical rotary encoder," *Elektronika Elektrotechnika*, vol. 26, no. 6, pp. 10–16, Dec. 2020.

Authorized licensed use limited to: Changchun Inst of Optics Fine Mechanics & Physics. Downloaded on February 07,2023 at 02:30:04 UTC from IEEE Xplore. Restrictions apply.

[10] J. Lopez and M. Artes, "A new methodology for vibration error compensation of optical encoders," *Sensors*, vol. 12, no. 4, pp. 4918–4933, Apr. 2012.
[11] H.-K. Jia, L.-D. Yu, Y.-Z. Jiang, H.-N. Zhao, and J.-M. Cao, "Compensation of rotary encoders using Fourier expansion-back propagation neural network optimized by genetic algorithm," *Sensors*, vol. 20, no. 9, pp. 4918–4933, May 2020.
[12] L. Iafolla, M. Filipozzi, S. Freund, A. Zam, G. Rauter, and P. C. Cattin, "Machine learning-based method for linearization and error compensation of a novel absolute rotary encoder," *Measurement*, vol. 169, Feb. 2021, Art. no. 108547.
[13] D. Gurauskis, A. Kilikevičius, and A. Kasparaitis, "Thermal and geometric error compensation approach for an optical linear encoder," *Sensors*, vol. 21, no. 2, p. 360, Jan. 2021.
[14] S. Wang, Z. Wu, D. Peng, S. Chen, Z. Zhang, and S. Liu, "Sensing mechanism of a rotary magnetic encoder based on time grating," *IEEE Sensors J.*, vol. 18, no. 9, pp. 3677–3683, May 2018.
[15] N. Anandan, A. V. Muppala, and B. George, "A flexible, planar-coil-based sensor for through-shaft angle sensing," *IEEE Sensors J.*, vol. 18, no. 24, pp. 10217–10224, Dec. 2018.
[16] H. Yu, X. Jia, Q. Wan, L. Liang, and C. Zhao, "High-resolution angular displacement technology based on varying Moiré figure phase positions," *IEEE Sensors J.*, vol. 19, no. 6, pp. 2126–2132, Mar. 2019.

**Changhai Zhao** (Member, IEEE) received the Ph.D. degree from the Changchun Institute of Optics, Fine Mechanics and Physics (CIOMP), Chinese Academy of Sciences, in 2008. He is currently an Associate Research Fellow with CIOMP, Chinese Academy of Sciences. His research interest includes electro-optical displacement precision measurement.

**Qiuhua Wan** was born in 1962. She is currently a Research Fellow with CIOMP, Chinese Academy of Sciences. Her research interest includes electro-optical displacement precision measurement.

**Xinran Lu** was born in 1978. He is currently an Associate Research Fellow with CIOMP, Chinese Academy of Sciences. His research interest includes electro-optical displacement precision measurement.

**Lihui Liang** was born in 1980. He is currently an Associate Research Fellow with CIOMP, Chinese Academy of Sciences. His research interest includes electro-optical displacement precision measurement.

Authorized licensed use limited to: Changchun Inst of Optics Fine Mechanics & Physics. Downloaded on February 07,2023 at 02:30:04 UTC from IEEE Xplore. Restrictions apply.